HHS Public Access

Author manuscript

J Biomed Mater Res B Appl Biomater. Author manuscript; available in PMC 2019 July 01.

Published in final edited form as:

J Biomed Mater Res B Appl Biomater. 2018 July ; 106(5): 1662–1671. doi:10.1002/jbm.b.33969.

Zeolite-loaded alginate-chitosan hydrogel beads as a topical hemostat

Parinaz Fathi[1,†], **Michael Sikorski**[1,2,†], **Katerina Christodoulides**[1], **Kristen Langan**[1], **Yoon Sun Choi**[1], **Michael Titcomb**[1], **Anjali Ghodasara**[1], **Omasiri Wonodi**[1], **Hemi Thaker**[1], **Mert Vural**[3], **Adam Behrens**[2], and **Peter Kofinas**[4]

[1]Gemstone Honors Program, University of Maryland, College Park, Maryland 20742

[2]Fischell Department of Bioengineering, University of Maryland, College Park, Maryland 20742

[3]Department of Materials Science and Engineering, University of Maryland, College Park, Maryland 20742

[4]Department of Chemical and Biomolecular Engineering, University of Maryland, College Park, Maryland 20742

Abstract

Hemorrhage is the leading cause of preventable death after a traumatic injury, and the largest contributor to loss of productive years of life. Hemostatic agents accelerate hemostasis and help control hemorrhage by concentrating coagulation factors, acting as procoagulants and/or interacting with erythrocytes and platelets. Hydrogel composites offer a platform for targeting both mechanical and biological hemostatic mechanisms. The goal of this work was to develop hydrogel particles composed of chitosan, alginate, and zeolite, and to assess their potential to promote blood coagulation via multiple mechanisms: erythrocyte adhesion, factor concentration, and the ability to serve as a mechanical barrier to blood loss. Several particle compositions were synthesized and characterized. Hydrogel bead composition was optimized to achieve the highest swelling capacity, greatest erythrocyte adhesion, and minimal *in vitro* cytotoxicity. These results suggest a polymer hydrogel-aluminosilicate composite material may serve as a platform for an effective hemostatic agent that incorporates multiple mechanisms of action.

Keywords

hemostatic; alginate; chitosan; zeolite; hydrogel

INTRODUCTION

Traumatic injury is the leading cause of death in the United States for people under the age of 44 and the fourth overall reported cause of death.[1] Two-thirds of trauma patients die prior to arrival at a hospital. Hemorrhage and associated shock accounts for 33 to 50% of all traumatic deaths.[2] This makes hemorrhage one of the largest contributors to the loss of

Correspondence to: P. Kofinas; kofinas@umd.edu.

†Indicates equal contribution.

productive years of life and places a heavy economic burden on communities.[3] It is also a primary cause of preventable death on the battlefield. Nearly 90% of military deaths are caused by hemorrhage, of which half are noncompressible.[4]

The body reacts to hemorrhage by undergoing a process called hemostasis. In primary (extrinsic) hemostasis, vasoconstriction rapidly occurs and damaged blood vessel cells release chemical signals to attract, activate, and aggregate platelets. Consequently, an initial platelet plug forms at the injury site. In secondary (intrinsic) hemostasis, coagulation protein factors are activated. In the final phase of this cascade, thrombin cleaves fibrinogen into fibrin, the main component of a blood clot, and a crosslinked network of fibrin is subsequently formed. The platelet plug and this fibrous network prevent further blood loss. Once blood loss has been stopped, healing begins and the fibrin clot is broken down via fibrinolysis.[5] If the body's hemostatic mechanisms are insufficient in controlling bleeding after traumatic injury, or a coagulopathy prevents normal hemostasis, intervention is required.

First responders in the emergency medical services and the military control external blood loss with standard protocols. Direct pressure is applied with sterile dressings to provide a physical barrier to blood loss and reduce perfusion to the injury site. Tourniquets, which can cause minor to extensive tissue death, are used when extremity bleeding cannot be treated with direct pressure.[6] If blood loss is uncontrollable at an injury site that is noncompressible (for example, torso) or inaccessible by a tourniquet (for example, axilla, neck, groin), then a hemostatic agent is necessary.

Hemostatic agents are materials that rapidly stop blood loss by augmenting one or more hemostatic mechanisms. These mechanisms include the concentration of clotting factors, direct activation of clotting factors via a procoagulant, and/or interactions with erythrocytes and platelets.[7,8] An ideal material should achieve hemostasis within minutes at an actively bleeding injury site and be ready for use, simple to apply, lightweight, durable, nonperishable when stored under all ambient conditions, safe, and inexpensive.[9] Although no currently available commercial product meets all of these criteria, several are approved for traumatic hemorrhage control in emergency and military settings. For example, approved by the Maryland Institute for Emergency Medical Services Systems for emergency first responder use are chitosan and aluminosilicate dressings.[10] Chitosan hemostatic dressings adhere to cell bodies and platelets, while aluminosilicate impregnated dressings rapidly absorb blood to concentrate clotting factors and act as a procoagulant.[11]

Chitosan is a polysaccharide commonly used in hemostatic dressings. It is a safe and readily available naturally derived material that binds with erythrocytes, activates macrophages, and stimulates cytokines.[12–15] Chitosan has also been shown to be an effective hemostatic agent when used in other forms, including chitosan-polyethylene glycol (PEG) tissue adhesives,[16] carboxymethyl chitosan microspheres,[17] and chitosan/gelatin sponges.[18]

Aluminosilicate minerals such as zeolite and kaolin are known for ultra-high water absorbance and local calcium release.[19] Zeolite is highly effective at promoting hemostasis through concentrating platelets and clotting factors by rapidly absorbing blood from the

injury site in an exothermic hydration reaction; however, the exothermic reaction can cause local tissue damage when zeolite is applied directly. This harmful side effect led commercial manufacturers to replace zeolite with kaolin. Kaolin absorbs blood with a lower entropy of hydration and increases coagulation by activating factor XII in the coagulation cascade.[20] Kaolin has also been coupled with zeolite to reduce the adverse side effects of zeolite while utilizing the effective attributes of the two aluminosilicates.[21]

The described research aims to develop an inexpensive and effective polymer hydrogel platform that incorporates the red blood cell adhesive properties of chitosan and high blood absorbance of zeolite, while mitigating negative effects of the exothermic hydration reaction and cytotoxicity. Alginate, a biocompatible polymer that crosslinks easily in the presence of calcium and has demonstrated swelling properties,[20–23] was selected to serve as a vehicle in which the positive effects of chitosan and zeolite could be combined. Studies focus on the synthesis, characterization, and *in vitro* assessment of hemostatic hydrogel beads of varying compositions of alginate, chitosan, and zeolite.

MATERIALS AND METHODS

Materials

Sodium alginate, zeolite (particle size < 45 μm), calcium chloride, acetic acid, and phosphate buffered saline (PBS, 1×) were purchased from Sigma-Aldrich (St. Louis, MO). Chitosan (MW 100–300 kDa) was purchased from Acros Organics (Fair Lawn, NJ). Ultra-pure deionized (DI) water was obtained from a Millipore Super-Q water system (Billerica, MA). Citrated sheep blood was purchased from Hemostat Laboratories (Dixon, CA) and was received and stored away from direct light at 3–88C following manufacturer's instructions. Blood was used within one week after arrival. Plastic-capped glass vials (5 mL) used in the study were purchased from VWR Scientific (West Chester, PA). Whole human blood for scanning electron microscopy (SEM) imaging was collected in several 2.7 mL citrate tubes at the University of Maryland Health Center in concordance with the University of Maryland Institutional Review Board [400316–3] titled "Zeolite Loaded Chitosan and Alginate Microparticles Designed for Hemostatic Use." MTS CellTiter 96® AQueous One Solution Cell Proliferation Assay (Promega, Madison, WI) and Live/Dead Cell Imaging Kit (Life Technologies, Carlsbad, CA), were used in cell viability testing. All materials were used as they were received unless otherwise described.

Synthesis and sizing of hydrogel beads

Hydrogel beads were prepared in a two-phase synthesis method adopted from a previously reported protocol with slight modification.[22] A 10 mL plastic syringe fitted with a 22.5 gauge needle was filled with the aqueous phase: 10 mL of alginate solution (4–6% w/v) and sodium zeolite powder (1:1 or 2:1 w/v zeolite-to-alginate ratio) in DI water. The syringe containing phase one solution was connected to an automated KDS100 Infusion Pump at a flow rate of 20 mL/hr and positioned 12 cm above a 150 mL glass beaker containing 80 mL of the second aqueous phase—1% (w/v) chitosan, 1% (w/v) $CaCl_2$, and 1% (w/v) acetic acid —under stirring at 300 rpm with a magnetic stir bar. The beads were transferred to a plastic 50 mL tube and rotated on a Labquake rotator to ensure total crosslinking. Within 3 days,

the beads were isolated via vacuum filtration, washed with DI water, and lyophilized using a Labconco FreeZone Triad Benchtop Freeze Dry System. The beads were frozen using liquid nitrogen and then freeze dried in the chamber at −558C under a 0.02 mBar vacuum. Different hydrogel bead compositions were synthesized by varying alginate 4–6% (w/v) and zeolite 4% or 8% (w/v). From this point forward, the primary compositions that were compared will be referred to as 4A0Z1C, 5A0Z1C, 6A0Z1C, 4A4Z1C, and 4A8Z1C, with the numbers before the letters “A,” “Z,” and “C” corresponding to the percentage of alginate, zeolite, and chitosan content in the synthesis solutions respectively. For further comparison and understanding, beads without chitosan and without both chitosan and acetic acid were also synthesized. All beads were lyophilized unless otherwise noted. Lyophilized 4A0Z1C, 4A4Z1C, and 4A8Z1C beads were imaged using an Axioskop 50 microscope equipped with an Axiocam color camera (Zeiss, Germany) and sized using ImageJ. 25–30 bead measurements of each composition were taken and sorted into 100 μm ranges. A size histogram was created to compare the size distribution.

Fourier transform infrared spectroscopy

A Fourier transform infrared (FTIR) spectrum was obtained for 4A4Z1C beads in a dried powder form. The spectrum was obtained on a Thermo Nicolet NEXUS 670 FTIR using a range of 500–4000 cm^{-1}.

Temporal swelling

Initial swelling studies were conducted with 4A0Z1C, 5A0Z1C, and 6A0Z1C beads. For each composition, 200 mg of beads were measured and added into preweighed 5 mL glass vials ($n = 6$). For each trial, 2 mL of 1× PBS was added to each of the vials. The vials were immediately placed on a vortex mixer for 10 s to break up aggregates, transferred to a Labquake rotator, and rotated until a designated time point of 5, 10, 30, or 60 min was reached. The excess PBS was then carefully removed by micropipette, after which the final weight of the vial was recorded, and the final swelled bead weight was calculated. Results were reported as a percent change in mass from the initial bead weight. Of the varying alginate compositions, 4A0Z1C beads demonstrated the greatest swelling and were selected for comparison with beads containing a 1:1 or 2:1 mass ratio of zeolite to alginate (4A4Z1C and 4A8Z1C, respectively). These bead compositions were tested at time points of 5 and 10 min using the same swelling procedure ($n = 3$).

In vitro particle stability

Mass loss from 4A0Z1C, 4A4Z1C, and 4A8Z1C beads was measured over 7 days under conditions of temperature, pH, and osmotic balance within physiological range of an acute injury site. 100 mg samples ($n = 3$) of each bead composition were added into preweighed 5 mL glass vials and submerged in 5 mL of 1× PBS. The samples were incubated at 378C and PBS was changed every 2 days. Each sample was dried under vacuum in a desiccator for 7 days, after which the dried weight was measured. Results were reported as a percent change in mass.

Scanning electron microscopy

Scanning electron microscopy imaging was conducted for 4A0Z1C desiccated, 4A0Z1C, 4A4Z1C, and 4A8Z1C beads. Beads were cut in half using a razor blade, and coated with carbon using an Electron Microscopy Sciences 150 T S Turbo-Pumped Sputter Coater/ Carbon Coater. Imaging was conducted with the core of each bead facing upward. Images were taken with a Hitachi SU-70 Schottky field emission gun scanning electron microscope using accelerating voltages ranging from 5 to 10 kV. Pore size was quantified using ImageJ. Each image was divided into four quadrants to account for variable brightness and images were analyzed one quadrant at a time. To begin, the image type was changed to an 8-bit image, and the background correction plugin was used with its default settings. Next, the image was sharpened and then made into a binary image. The image was then inverted, such that the dark spots corresponded to the location of pores. Finally, pore area was determined using the particle analysis tool. A threshold area of 0.002 μm^2 was used to account for noise.

SEM experiments with citrated blood were conducted to observe citrated whole blood adhesion and interaction with 4A0Z0C, 4A0Z1C, and 4A4Z1C beads. For each bead composition, 100 mg of beads were placed into a 5 mL glass vial. 1 mL of fresh human whole blood was added to the vial, and the vial was placed on a Labquake rotator for 5 min. The sample was then removed from the vial and placed in a sample cassette to be washed. The sample was rinsed four times, each time with 10 mL of PBS, and then fixed in 25 mL of 0.025 M glutaraldehyde for an hour. The sample was then washed four more times in 10 mL of PBS to remove glutaraldehyde. A series of ethanol solutions of increasing concentration were applied to the washed sample. The series consisted of 25%, 50%, 70%, 95%, and 100% ethanol. The sample was stored in a desiccator and then coated with carbon and imaged with a Hitachi SU-70 Schottky field emission gun scanning electron microscope.

Heparinized blood experiments were conducted to observe heparinized whole blood adhesion and interaction with 4A4Z1C beads, following the same protocol for citrated blood. Samples were coated with carbon and imaged with a JEOL JSM-6390LV scanning electron microscope with an accelerating voltage of 10 kV.

Coagulation time

Following a previously established protocol,[23] coagulation times of varying bead or material compositions were tested in 5 mL glass vials ($n = 3$). Four percent of citrated whole sheep blood stored for no more than one week away from direct light at 3–88C was warmed to room temperature just prior to use in this experiment. Blood was not warmed to 378C prior to use in order to avoid the temporal effects of cooling on coagulation time. 1 mL of room temperature 4% citrated whole sheep blood was recalcified using a 0.2 M $CaCl_2$ stock to achieve a final $CaCl_2$ concentration of 10 mM, vortexed, and added to each sample. Bead samples were prepared in volumes equivalent to the volume of 150 mg of 4A1Z1C beads. Each vial was capped and examined for coagulation by inversion. Coagulation was defined as when the entire sample was stagnant during inversion. If coagulation did not occur immediately, each vial was set on a Lab-quake rotator for 1 min. After a minute, each vial was removed from the rotator and examined again for coagulation. This procedure was repeated until coagulation was induced in each sample, in which the blood ceased to flow.

Cell viability

L929 murine fibroblast cells (Lonza) suspended in DMEM were added to a sterile 24-well cell culture plate. Cells were then incubated at 378C and 5% CO_2 for 48 hours until 100% confluency was reached. After 48 hours, samples ($n = 3$) of 4A0Z1C, 4A4Z1C, and 4A8Z1C beads were sterilized under UV light and added on top of the plated cells such that 10–15% of the well surface area was covered by beads. Plated cells with DMEM served as a live control and cells treated with a 70% solution of methanol for 30 min served as a dead control. At 72 hours, an MTS proliferation assay (absorbance read at 490 nm) and a Live/Dead assay were performed separately following each manufacturer's instructions.

Statistical analysis

Data is reported as the mean ± standard deviation, unless otherwise noted. Significance for all data was analyzed using a one-way analysis of variance (ANOVA) followed by a Tukey HSD test, and reported as $p < 0.05$, $p < 0.01$, or $p < 0.001$.

RESULTS

Synthesis and sizing of zeolite-loaded alginate-chitosan beads

Hydrogel bead compositions were synthesized following a two-phase synthesis method (Figure 1). Synthesized compositions are summarized in Table I. The average 4A0Z1C bead size was 1536 ± 96 μm, the average 4A4Z1C bead size was 1693 ± 85 μm, and the average 4A8Z1C bead size was 1636 ± 112 μm [Figure 2(A–C)].

Fourier transform infrared spectroscopy

The FTIR spectrum [Figure 2(D)] for the 4A4Z1C beads displays absorbance peaks of N-H stretching and O-H stretching (broad band at ~3359 cm^{-1}), in addition to C-H stretching at ~2927 cm^{-1}. It also displays an Amide II bending vibration and carboxylate group asymmetric stretching (both at ~1602 cm^{-1}), as well as carboxylate group symmetric stretching (~1425 cm^{-1}). The peak at ~1033 cm^{-1} corresponds to C-O stretching and SiO_4 tetrahedral stretching.

Temporal swelling

The average change in mass for the 4A0Z1C, 5A0Z1C, and 6A0Z1C beads was plotted over 1 hour [Figure 2(E)]. The 4A0Z1C beads showed the greatest average change in mass at each time point, followed by 5A0Z1C, and then 6A0Z1C beads. At one hour, 4A0Z1C, 5A0Z1C, and 6A0Z1C beads displayed an average percent change in mass of approximately 394% (± 40% standard error), 307% (± 31% standard error), and 180% (± 34% standard error) respectively.

The average percent change in mass for 4A0Z1C, 4A4Z1C, and 4A8Z1C beads at the 5 and 10 min time points is displayed in Figure 2(F). The addition of zeolite in a 1:1 zeolite:alginate ratio increased the change in mass at the 5 and 10 min time points (359 ± 15% standard error and 372 ± 8% standard error respectively) compared to the change in mass of the 4A0Z1C beads (280 ± 13% standard error and 293 ± 13% standard error respectively). The addition of a 2:1 ratio of zeolite decreased the change in mass at the 5 and

10 min time points (223 ± 20% standard error and 201 ± 8% standard error) compared to the change in mass of the 4A0Z1C and 4A4Z1C beads.

In vitro particle stability

4A0Z1C, 4A4Z1C, and 4A8Z1C beads were evaluated over 7 days under conditions of temperature, pH, and osmotic balance within normal physiological range for changes in mass [Figure 2(G)]. Incubation of 4A0Z1C, 4A4Z1C, and 4A8Z1C beads in 378 C conditions for 7 days yielded an average loss of mass of 12.76% (± 3.66%), 68.36% (± 2.56%), and 22.84% (± 2.68%), respectively. Average change of mass was obtained by subtracting the final desiccated mass of each set of beads from the initial lyophilized mass before the addition of 1× PBS.

Scanning electron microscopy

SEM images were obtained of the cores of 4A0Z1C desiccated, 4A0Z1C, 4A4Z1C, and 4A8Z1C beads [Figure 3(A–D)]. Visual observation of these images shows smaller pores in the 4A0Z1C desiccated beads compared to the lyophilized beads. The 4A0Z1C desiccated beads had the smallest average pore area (0.00899 ± 0.0024 μm^2 standard error) followed by 4A8Z1C (0.0457 ± 0.012 μm^2 standard error), 4A0Z1C (0.133 ± 0.030 μm^2 standard error), and 4A4Z1C (0.194 ± 0.056 μm^2 standard error) [Figure 3(E)].

SEM images were obtained of 4A0Z0C, 4A0Z1C, and 4A4Z1C beads treated with citrated blood (Figure 4). The 4A4Z1C beads displayed the greatest amount of erythrocyte adhesion, followed by the 4A0Z1C and 4A0Z0C beads.

SEM images were obtained of 4A4Z1C beads treated with heparinized blood (Figure 5). The 4A4Z1C beads displayed surface erythrocyte adhesion despite the use of heparinized blood.

Coagulation time

Coagulation of whole sheep blood induced by various bead compositions and materials was evaluated (Figure 6). The control of recalcified whole sheep blood reached coagulation at an average of 9 min (9.11 ± 0.11 min). The 4A4Z1C and 4A8Z1C beads induced coagulation in under 15 seconds (14.4 ± 0.31 sec and 14.76 ± 1.36 sec, respectively). In comparison, the 4A0Z1C beads induced coagulation in under 2 min (1.96 ± 0.14 min). The 4A0Z0C beads reached full coagulation in under 5.5 min (5.22 ± 0.32 min).

Cell Viability

ISO 10993–5:2009(E) quantifies a cytotoxic effect as a reduction of cell viability by >30% to a value <70% of the live control.[24] Fluorescent microscopy was used to visualize the Live/Dead Cell Assay which showed dead cells as red and live cells as green [Figure 7(A)]. The 4A0Z1C, 4A4Z1C, and 4A8Z1C beads performed comparably, each showing high cell viability >70% according to ISO 10993–5:2009(E). Separately, in the MTT assay, the 4A4Z1C and 4A0Z1C bead groups both demonstrated greater cell metabolic activity than the live control. The 4A0Z1C beads had 110.3% (± 6.63% standard error) of the metabolic activity of the live control [Figure 7(B)] and the 4A4Z1C beads had 118.9% (± 3.67% standard error) of the metabolic activity of the live control [Figure 7(C)]. The 4A8Z1C beads

[Figure 7(D)] and zeolite-only groups [Figure 7(E)] had lower metabolic activity than the live control (80.4 ± 3.77% and 23.4 ± 9.08%, respectively). Following ISO 10993–5:2009(E) the zeolite-only group is cytotoxic.

DISCUSSION

This work utilized a hydrogel that targets multiple mechanisms to promote blood coagulation. The composition was designed to take advantage of chitosan's ability to adhere to red blood cells and platelets, zeolite's blood absorbance to concentrate clotting factors, and alginate's porous structure to absorb and retain fluid while acting as a physical barrier to blood loss.

Synthesis and characterization

A two-phase synthesis method utilizing a syringe pump was used to synthesize a wide range of bead compositions (Table I). The beads were observed to have a spherical morphology. SEM images were taken to compare the pore size of 4A0Z1C beads dried using desiccation and lyophilization, finding that lyophilized beads had a greater pore size than desiccated beads. The differences in pore size observed in each case reflect the differences between the chosen drying methods, with lyophilization, which removes the water from hydrogels through sublimation, preserving the porous structure of the beads. Larger pore sizes within the range reported here –an area of 0.009 to 0.194 μm^2, corresponding to a diameter of about 50–250 nm –in semisynthetic alginate polymer hydrogels of comparable bead diameter was associated with a higher swelling ratio of ionic saline solutions at physiological pH and temperature.[25] Hydrogel beads with a high swelling ratio enable local concentration of clotting factors and can serve as a physical barrier to blood loss.[23] Consequently, lyophilization was chosen as the drying method for the beads used in further experiments. Swelling data for comparison of lyophilized and desiccated beads is provided in the Supporting Information.

The average bead size for 4A0Z1C (1536 ± 96 μm) was found to be less than that of the 4A4Z1C (1693 ± 85 μm) and 4A8Z1C (1636 ± 112 μm), indicating that the incorporation of zeolite increased bead size. These small differences were not expected to greatly impact blood-material interaction. FTIR spectroscopy was used to confirm the presence of alginate, chitosan, and zeolite in the 4A4Z1C bead composition according to previous reports in literature. The broad absorbance peaks of N-H stretching and O-H stretching at ~3359 cm^{-1} indicate the polyelectrolyte complexes formed between chitosan and alginate.[26] The C-H stretching peak at ~2927 cm^{-1} corresponds to chitosan, and the peak at ~1602 cm^{-1} corresponds to the chitosan Amide II bending vibration and alginate carboxylate group asymmetric stretching.[26–29] The presence of alginate carboxylate group symmetric stretching is indicated by the peak at ~1425 cm^{-1}.[27,30] The peak at ~1033 cm^{-1} corresponds to C-O stretching from alginate[27] and the SiO_4 tetrahedral structure of zeolite.[31] This confirmed that all expected components were incorporated into the beads during the fabrication process.

Beads with varying concentrations of alginate and zeolite were then characterized to determine the composition with the greatest swelling and largest pore diameters. As alginate

concentration was increased from 4% to 6%, temporal swelling decreased. This is likely due to an increased amount of crosslinking occurring as the alginate concentration is increased, therefore allowing for less expansion during water uptake.[32,33] The effect of zeolite content on swelling was assessed by comparing 4A0Z1C beads with 4A4Z1C and 4A8Z1C beads. The addition of the 1:1 ratio of zeolite was associated with the largest increase in swelling, likely due to zeolite's high water absorbance. However, the addition of the 2:1 ratio of zeolite was found to decrease swelling. This may have been caused by the increased density of 4A8Z1C beads compared to the 4A0Z1C and 4A4Z1C beads. The effects of zeolite concentration on swelling were further supported by the quantitative analysis of the pore sizes of 4A0Z1C, 4A4Z1C, and 4A8Z1C from SEM images, which found that the 4A4Z1C beads had the greatest average pore area while the 4A8Z1C beads had the smallest average pore area. The larger pore area of the 4A4Z1C beads should allow for absorption of a greater volume of fluid, or blood, and in turn yield enhanced hemostatic properties due to greater concentration of local clotting factors.

Mass loss from 4A0Z1C, 4A4Z1C, and 4A8Z1C beads was evaluated after seven days under conditions representing normal physiological temperature, pH, and osmotic balance, with the 4A4Z1C beads exhibiting a much greater mass loss than the 4A0Z1C beads, and the 4A8Z1C beads exhibiting an intermediate level of mass loss. The higher swelling and larger pore size in the 4A4Z1C beads may have led to the absorbance of a greater quantity of PBS, as well as a larger pore surface area within which solvent-material interactions could occur. The simulated conditions did not take into account potential oxidative degradation of the hydrogels *in situ* due to the local release of peroxides and reactive oxygen species (ROS) from neutrophils and macrophages during the inflammatory response to an foreign body.[34] Oxidative degradation due to local inflammation would likely accelerate the rate of degradation of the zeolite loaded alginate-chitosan hydrogel beads, but to what extent is uncertain given that calcium chloride crosslinked 3% w/v alginate hydrogel beads have previously shown low induction of ROS and very little tissue response when implanted in live animals.[35]

In vitro interaction with whole blood

The different bead compositions were evaluated using a time to coagulation study. The 4A4Z1C beads and 4A8Z1C beads took the shortest time to induce coagulation. This is likely due to the combination of the electrostatic properties of chitosan and increased blood absorbance through the inclusion of zeolite. Chitosan interacts with the cell membranes of erythrocytes, allowing for rapid clot formation.[12] Moreover, zeolite's ability to absorb blood through its porous structure concentrates clotting factors and accelerates fibrin formation and platelet activation.[19] As each of the above components was removed, the means by which the beads induced coagulation was impeded, resulting in a greater time to coagulation for the beads that lacked zeolite or both zeolite and chitosan. The similarity in coagulation time of the 4A4Z1C and 4A8Z1C beads, in conjunction with their differences in temporal swelling, suggest that at short time scales relevant to hemostasis, each of these bead compositions reach sufficient swelling levels to promote coagulation. Notably, the coagulation experiment was completed using blood warmed to room temperature, rather than to 378C. The chosen experimental temperature should not have impacted the results

because temperature uniformly affects the rate of coagulation, with the time to coagulation shortening as temperature rises from about 108C to 408C, after which the time is prolonged and ultimately infinite.[36] These *in vitro* results demonstrate the promising capacity of a composite hydrogel biomaterial to augment the intrinsic (secondary) hemostatic cascade; however, *in vitro* studies are limited in their assessment to this pathway and do not replicate the extrinsic clotting cascade, which is often viewed as the primary mechanism of hemostasis. These effects will have to be further studied *in vivo*.

The SEM experiments with citrated blood further confirmed the role of each bead component in coagulation. The 4A0Z0C beads displayed little to no erythrocyte adhesion, which was likely due to the absence of chitosan. The addition of chitosan to the beads took advantage of chitosan's adhesive properties as displayed by the moderate erythrocyte adhesion in the 4A0Z1C beads. Finally, the addition of zeolite resulted in the greatest erythrocyte adhesion in the 4A4Z1C beads, which suggests that the combination of chitosan's adhesive properties and zeolite's high blood absorbance both contributed to the efficacy of the beads. Zeolite's blood absorbance may have concentrated erythrocytes in the regions immediately surrounding the beads, leading to the increased erythrocyte adhesion on the bead surface. This erythrocyte aggregation effect has been previously observed when whole blood came into contact with a hemostatic agent that employs kaolin, a similar aluminosilicate.[37]

Erythrocyte adhesion in the citrated blood SEM experiments suggested that coagulation may have begun upon contact with the beads, despite the use of a calcium-sequestering anticoagulant. It is possible that the beads reintroduced calcium into the citrated blood. The system was therefore additionally evaluated using heparinized blood. Despite the change in anticoagulant, erythrocytes adhered to the 4A4Z1C bead surfaces, reaffirming the ability of the hydrogel beads to cause erythrocyte adhesion.

Thus, the zeolite-loaded beads were found not only to be effective in clotting recalcified blood, but also to be effective in causing erythrocyte adhesion in both citrated and heparinized whole blood. The major limitation of these results is that they do no investigate the behavior of other clotting factors or the aggregation and activation platelets. Further work would need to be conducted in order to evaluate the effects of these hydrogel beads on other major clotting mechanisms.

Cell viability

The live/dead cell viability assay qualitatively demonstrated that the 4A0Z1C, 4A4Z1C, and 4A8Z1C beads performed comparably, inducing only some cell death, whereas the cells treated with zeolite alone appeared comparable to the dead control. This suggests that the negative side effects of zeolite might be mitigated through its incorporation into hydrogel beads. This is further suggested by the MTS assay, which showed that the 4A4Z1C beads had the greatest metabolic activity, followed by the 4A0Z1C beads, the 4A8Z1C beads, and the zeolite alone. The slightly elevated fibroblast metabolic activity in response to the 4A4Z1C beads may indicate an elevated cellular stress response to the introduction of a low level of zeolite. Zeolite and other aluminosilicates have been previously shown to have cytotoxic effects when in direct contact with cells normally present at the site of injury.[38]

When zeolite content was doubled in the 4A8Z1C beads, it is possible that the damaging effects of zeolite in direct contact with cells overcame the mitigating ability of the composite bead and resulted in depressed metabolic output, confirming previous reports of the negative effects of zeolite. The improved performance of 4A4Z1C beads compared to the 4A8Z1C beads might suggest that although zeolite can illicit negative side effects, if used in certain amounts alongside alginate and chitosan it may be both effective as a hemostatic agent and safer than zeolite alone.

CONCLUSION

Hydrogel particles composed of chitosan and alginate and loaded with zeolite were synthesized and their chemical, mechanical, and physical properties were characterized. Synthesized beads of varying composition were found to have a narrow size distribution with average diameters ranging from 1536 to 1693 μm. Chemical composition of the beads was confirmed using FTIR. The 4A4Z1C beads exhibited the greatest swelling capacity of all examined compositions and degraded significantly more than 4A0Z1C beads. When introduced to whole sheep blood during *in vitro* studies, the 4A4Z1C beads induced blood coagulation in under 15 seconds, as compared to 9 min for the control samples of whole sheep blood. SEM imaging of beads exposed to citrated human whole blood revealed the highest erythrocyte adhesion on 4A4Z1C beads, with progressively less adhesion on 4A0Z1C, and 4A0Z0C beads respectively. SEM images of 4A4Z1C beads exposed to heparinized human whole blood demonstrated erythrocyte adhesion despite the use of an anticoagulant that does not interact with calcium. An MTS proliferation assay and a live/dead assay suggested that 4A4Z1C particles had minimal impact on viability and metabolic activity, suggesting that the damaging direct effects of zeolite may be mitigated through the use of composite beads.

The beads developed in this study offer a potential platform for an affordable, accessible, and effective hemostatic agent for use in treatment of traumatic hemorrhage. This study demonstrates the plausibility of incorporating multiple mechanisms of action into a hemostatic agent. The major mechanisms that were targeted included the adhesive properties of chitosan and the blood absorbance of zeolite. Further research should be completed to identify and quantify the material's impact on specific primary and secondary hemostatic pathways, and to assess its biocompatibility and hemostatic performance in injury models.

Acknowledgments

We would like to acknowledge May Bayomi, Jocelyn Knazik, Benjamin Miller and Leopoldo Torres for their contributions to various aspects of this work. We would like to thank Dr. Silvia Muro and Zois Tsinas for their assistance with lyophilization, and Dr. John Fisher for his experimental assistance. We would like to acknowledge the Gemstone Program at the University of Maryland for supporting this research as well as the Maryland NanoCenter.

Contract grant sponsor: Howard Hughes Medical Institute Gemstone Research

Grant Contract grant sponsor: A.M.B. was supported by the National Institute of Biomedical Imaging and Bioengineering of the National Institutes of Health; contract grant numbers: F31EB019289; R01EB019963

Abbreviations

ANOVA	analysis of variance
DI	deionized
FTIR	Fourier transform infrared
MW	molecular weight
PBS	phosphate buffered saline
PEG	polyethylene glycol
ROS	reactive oxygen species
SEM	scanning electron microscopy

References

1. Centers for Disease Control and Prevention. Web-based injury statistics query and reporting system (WISQARS) [Internet]. U.S. Department of Health and Human Services, CDC, National Center for Injury Prevention and Control; 2014. Available from: www.cdc.gov/injury/wisqars/index.html
2. Evans JA, van Wessem KJP, McDougall D, Lee KA, Lyons T, Balogh ZJ. Epidemiology of traumatic deaths: Comprehensive population-based assessment. World J Surg. 2009; 34:158–163.
3. Kauvar DS, Lefering R, Wade CE. Impact of hemorrhage on trauma outcome: An overview of epidemiology, clinical presentations, and therapeutic considerations. J Trauma-Inj Infect Crit Care. 2006; 60:S3–S9.
4. Kelly JF, Ritenour AE, McLaughlin DF, Bagg KA, Apodaca AN, Mallak CT, Pearse L, Lawnick MM, Champion HR, Wade CE, Holcomb JB. Injury severity and causes of death from Operation Iraqi Freedom and Operation Enduring Freedom: 2003–2004 versus 2006. J Trauma. 2008; 64(S21):26–27.
5. Keohane, E., Smith, L., Walenga, J. Overview of Hemostasis Rodak's Hematology: Clinical Principles and Applications. 5th. St. Louis, Missouri: Elsevier Health Sciences; 2015.
6. Kragh JF, Swan KG, Smith DC, Mabry RL, Blackbourne LH. Historical review of emergency tourniquet use to stop bleeding. Am J Surg. 2012; 203:242–252. [PubMed: 21782152]
7. Granville-Chapman J, Jacobs N, Midwinter MJ. Pre-hospital haemostatic dressings: A systematic review. Injury. 2011; 42:447–459. [PubMed: 21035118]
8. Behrens AM, Sikorski MJ, Kofinas P. Hemostatic strategies for traumatic and surgical bleeding. J Biomed Mater Res A. 2014; 102:4182–4194. [PubMed: 24307256]
9. Pusateri AE, Holcomb JB, Kheirabadi BS, Alam HB, Wade CE, Ryan KL. Making sense of the preclinical literature on advanced hemostatic products. J Trauma. 2006; 60:674–682. [PubMed: 16531876]
10. The Maryland Medical Protocols for Emergency Medical Services Providers [Internet]. Maryland Institute for Emergency Medical Services Systems. 2016. Available from: http://www.miemss.org/
11. Achneck HE, Sileshi B, Jamiolkowski RM, Albala DM, Shapiro ML, Lawson JH. A Comprehensive review of topical hemostatic agents: Efficacy and recommendations for use. Ann Surg. 2010; 251:217–228. [PubMed: 20010084]
12. Baldrick P. The safety of chitosan as a pharmaceutical excipient. Regul Toxicol Pharmacol. 2010; 56:290–299. [PubMed: 19788905]
13. Chan LW, Kim CH, Wang X, Pun SH, White NJ, Kim TH. Poly-STAT-modified chitosan gauzes for improved hemostasis in external hemorrhage. Acta Biomater. 2016; 31:178–185. [PubMed: 26593785]

14. Kozen BG, Kircher SJ, Henao J, Godinez FS, Johnson AS. An alternative hemostatic dressing: Comparison of CELOX, HemCon, and QuikClot. Acad Emerg Med. 2008; 15:74–81. [PubMed: 18211317]
15. Burkatovskaya M, Tegos GP, Swietlik E, Demidova TN, P Castano A, Hamblin MR. Use of chitosan bandage to prevent fatal infections developing from highly contaminated wounds in mice. Biomaterials. 2006; 27:4157–4164. [PubMed: 16616364]
16. Lih E, Lee JS, Park KM, Park KD. Rapidly curable chitosan-PEG hydrogels as tissue adhesives for hemostasis and wound healing. Acta Biomater. 2012; 8:3261–3269. [PubMed: 22617740]
17. Liu L, Lv Q, Zhang Q, Zhu H, Liu W, Deng G, Wu Y, Shi C, Li H, Li L. Preparation of carboxymethyl chitosan microspheres and their application in hemostasis. Disaster Med Public Health Prep. 2015:1–8. [PubMed: 25901335]
18. Lan G, Lu B, Wang T, Wang L, Chen J, Yu K, Liu J, Dai F, Wu D. Chitosan/gelatin composite sponge is an absorbable surgical hemostatic agent. Colloids Surf B Biointerfaces. 2015; 136:1026–1034. [PubMed: 26590895]
19. Li J, Cao W, Lv X, Jiang L, Li Y, Li W, Chen S, Li X. Zeolite-based hemostat QuikClot releases calcium into blood and promotes blood coagulation *in vitro*. Acta Pharmacol Sin. 2013; 34:367–372. [PubMed: 23334236]
20. Arnaud F, Tomori T, Carr W, McKeague A, Teranishi K, Prusaczyk K, McCarron R. Exothermic reaction in zeolite hemostatic dressings: QuikClot ACS and ACS+ Ann Biomed Eng. 2008; 36:1708–1713. [PubMed: 18712606]
21. Zhang Y, Xu C, He Y, Wang X, Xing F, Qiu H, Liu Y, Ma D, Lin T, Gao J. Zeolite/polymer composite hollow microspheres containing antibiotics and the *in vitro* drug release. J Biomater Sci Polym Ed. 2011; 22:809–822. [PubMed: 20566060]
22. Bajpai SK, Tankhiwale R. Investigation of water uptake behavior and stability of calcium alginate/chitosan bi-polymeric beads: Part-1. React Funct Polym. 2006; 66:645–658.
23. Behrens AM, Sikorski MJ, Li T, Wu ZJ, Griffith BP, Kofinas P. Blood-aggregating hydrogel particles for use as a hemostatic agent. Acta Biomater. 2014; 10:701–708. [PubMed: 24185001]
24. ISO. Int Stand ISO 10993 [Internet]. 3rd. Geneva, Switzerland: International Organization for Standardization; 2009. 10993–5:2009(E) Biological evaluation of medical devices — Part 5: Tests for *in vitro* cytotoxicity. Available from: www.iso.org
25. Chan AW, Neufeld RJ. Modeling the controllable pH-responsive swelling and pore size of networked alginate based biomaterials. Biomaterials. 2009; 30:6119–129. [PubMed: 19660810]
26. Hu Z, Hong P, Liao M, Kong S, Huang N, Ou C, Li S. Preparation and characterization of chitosan—agarose composite films. Materials. 2016; 9:816.
27. Król Ż, Malik M, Marycz K, Jarmoluk A. Characteristic of gelatine, carrageenan and sodium alginate hydrosols treated by direct electric current. Polymers. 2016; 8:275.
28. Luo Y, Zhou Z, Yue T. Synthesis and characterization of nontoxic chitosan-coated Fe3O4 particles for patulin adsorption in a juice-pH simulation aqueous. Food Chem. 2017; 221:317–323. [PubMed: 27979209]
29. Wang X, Tang R, Zhang Y, Yu Z, Qi C. Preparation of a novel chitosan based biopolymer dye and application in wood dyeing. Polymers. 2016; 8:338.
30. Xiao Q, Gu X, Tan S. Drying process of sodium alginate films studied by two-dimensional correlation ATR-FTIR spectroscopy. Food Chem. 2014; 164:179–184. [PubMed: 24996322]
31. Byrappa K, Suresh Jumar BB. Characterization of zeolites by infrared spectroscopy. Asian J Chem. 2007; 19:4933–4935.
32. Xie L, Jiang M, Dong X, Bai X, Tong J, Zhou J. Controlled mechanical and swelling properties of poly(vinyl alcohol)/sodium alginate blend hydrogels prepared by freeze–thaw followed by Ca2+ crosslinking. J Appl Polym Sci. 2012; 124:823–831.
33. Giridhar RS, Pandit AS. Effect of curing agent on sodium alginate blends using barium chloride as crosslinking agent and study of swelling, thermal, and morphological properties. Int J Polym Mater Polym Biomater. 2013; 62:743–748.
34. Lugrin J, Rosenblatt-Velin N, Parapanov R, Liaudet L. The role of oxidative stress during inflammatory processes. Biol Chem. 2013; 395:203–230.

35. Liu WF, Ma M, Bratlie KM, Dang TT, Langer R, Anderson DG. Real-time *in vivo* detection of biomaterial-induced reactive oxygen species. Biomaterials. 2011; 32:1796–1801. [PubMed: 21146868]

36. Simpson S, Rasmussen AT. The effect of temperature on blood coagulation time. Q J Exp Physiol. 1916; 10:159–168.

37. Szymonowicz M, Kucharska M, Wi sniewska-Wrona M, Dobrzynski M, Kołodziejczyk K, Rybak Z. The evaluation of resorbable haemostatic wound dressings in contact with blood *in vitro*. Acta Bioeng Biomech. 2017; 19:151–165. [PubMed: 28552917]

38. Bowman P, Wang X, Meledeo M, Dubick M, Kheirabadi B. Toxicity of aluminum silicates used in hemostatic dressings toward human umbilical veins endothelial cells, hela cells, and RAW267.4 mouse macrophages. J Trauma-Inj Infect Crit Care. 2011; 71:727–732.

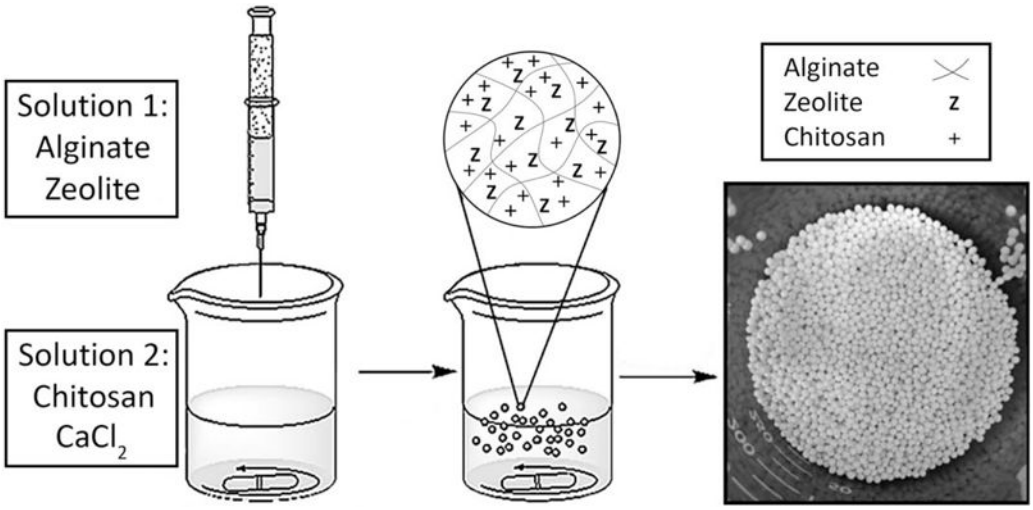

FIGURE 1.
Hydrogel bead synthesis schematic.

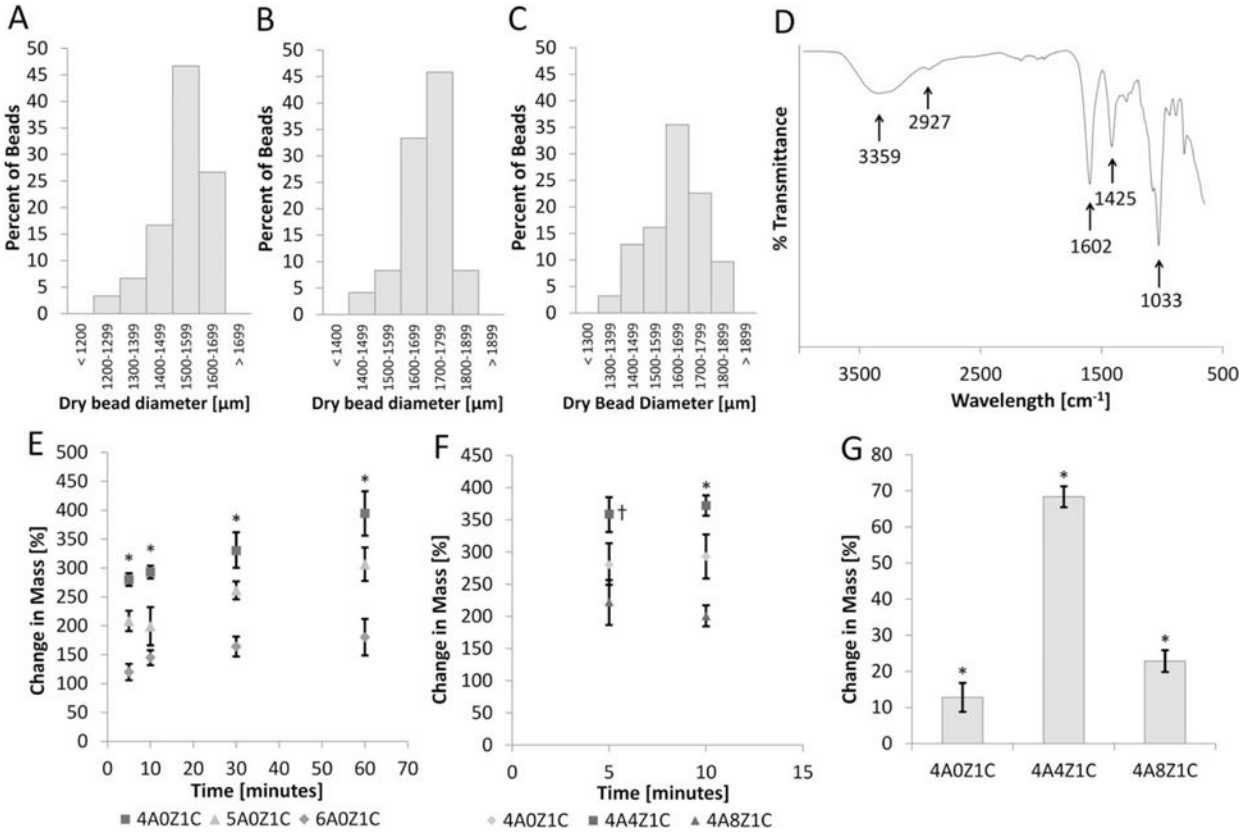

FIGURE 2.

Sizing, FTIR, swelling, and mass loss. Bead sizes for (A) 4A0Z1C, (B) 4A4Z1C, and (C) 4A8Z1C are organized into bins with 100 μm ranges based on image analysis. (D) FTIR data for 4A4Z1C beads show absorbance peaks of N-H and O-H (broad band at ~3359 cm^{-1}), O-H stretching (~2927 cm^{-1}), C = O (~1602 cm^{-1}), COOH (~1425 cm^{-1}), SiO_4 tetrahedral stretching (~1033 cm^{-1}). (E) The average changes in mass of 4A0Z1C, 5A0Z1C, and 6A0Z1C beads are compared over one hour. Error bars show standard error. (F) The average changes in mass of 4A4Z1C and 4A8Z1C beads are compared at times pertinent to hemostasis. Error bars show standard error. (G) Mass loss in physiological conditions is assessed after 7 days. The error bar shows standard deviation. * indicates $p < 0.05$ compared within time points or between groups. † indicates $p < 0.05$ for group 4A4Z1C compared with both other groups.

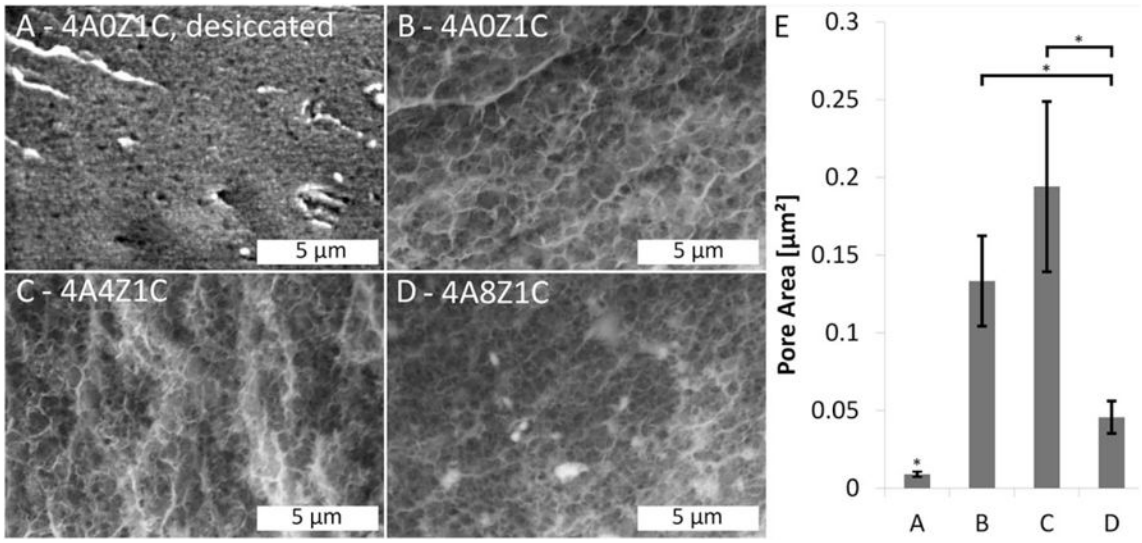

FIGURE 3.

SEM imaging of pores. A SEM image of a (A) 4A0Z1C, dried via desiccation; displaying relatively small pore size, (B) 4A0Z1C, displaying relatively large pore size, (C) 4A4Z1C, displaying a relatively large pore size and, (D) 4A8Z1C, displaying moderate pore size. (E) Average pore size of the corresponding compositions A–D calculated using image analysis of SEM images as described in the methods. For this analysis, images were divided into quadrants and analyzed one quadrant at a time in ImageJ. Images were converted to 8-bit format, and the background correction plugin was applied, followed by image sharpening and conversion to a binary image. Pore area was then determined using the particle analysis tool, with a threshold area of 0.002 μm^2 used to account for noise. Error bars show standard error. * indicates $p < 0.05$ compared between groups.

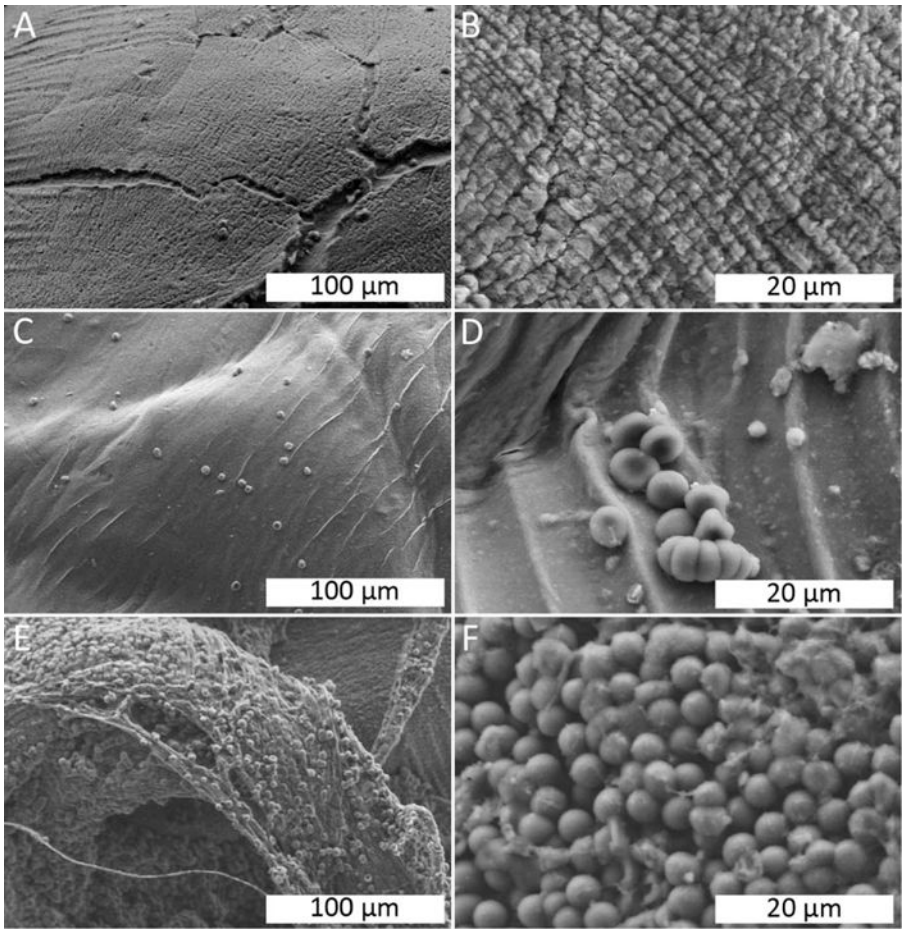

FIGURE 4.

SEM imaging of beads in citrated whole blood. (A) 4A0Z0C, showing minimal cell adhesion. (B) 4A0Z0C, showing a striated surface, but no cell adhesion. (C) 4A0Z1C, showing a smooth surface and sparse amounts of erythrocyte adhesion. (D) 4A0Z1C, showing a small cluster of erythrocytes adhering to the bead's surface. (E) 4A4Z1C, showing complete coverage of erythrocytes on the surface of the bead along with the presence of fibrous structures. (F) 4A4Z1C, showing a layer of erythrocytes covering the bead's surface.

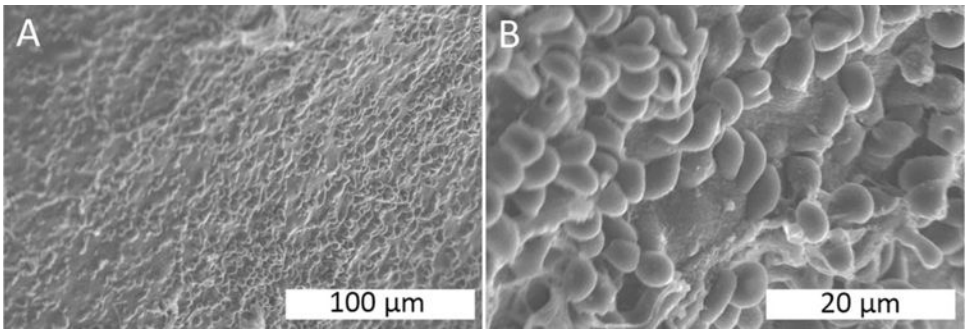

FIGURE 5.
SEM imaging of beads in heparinized whole blood. (A–B) 4A4Z1C, showing high erythrocyte adhesion.

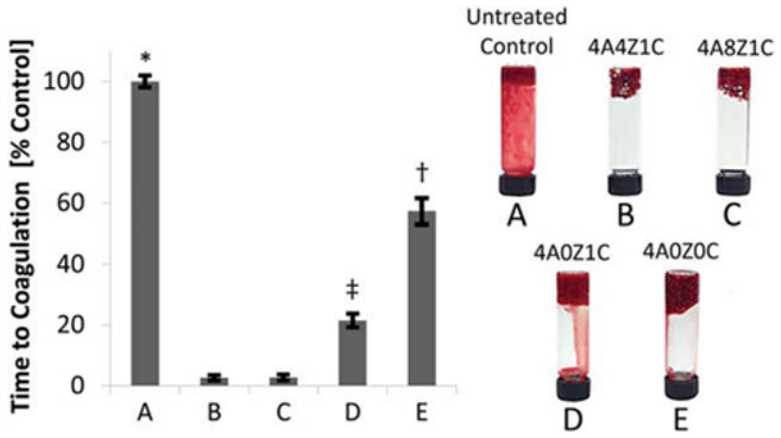

FIGURE 6.

Blood coagulation. Comparison of coagulation times in ovine whole blood as a percentage of an untreated control for five different bead compositions—(A) untreated control, (B) 4A4Z1C, (C) 4A8Z1C, (D) 4A0Z1C, (E) 4A0Z0C. Coagulation did not occur with pure zeolite. Error bars represent standard deviation. * indicates $p < 0.001$ for group A compared with all other groups. † indicates $p < 0.001$ for group E compared with all other groups. ‡ indicates $p < 0.001$ for group D compared with all other groups.

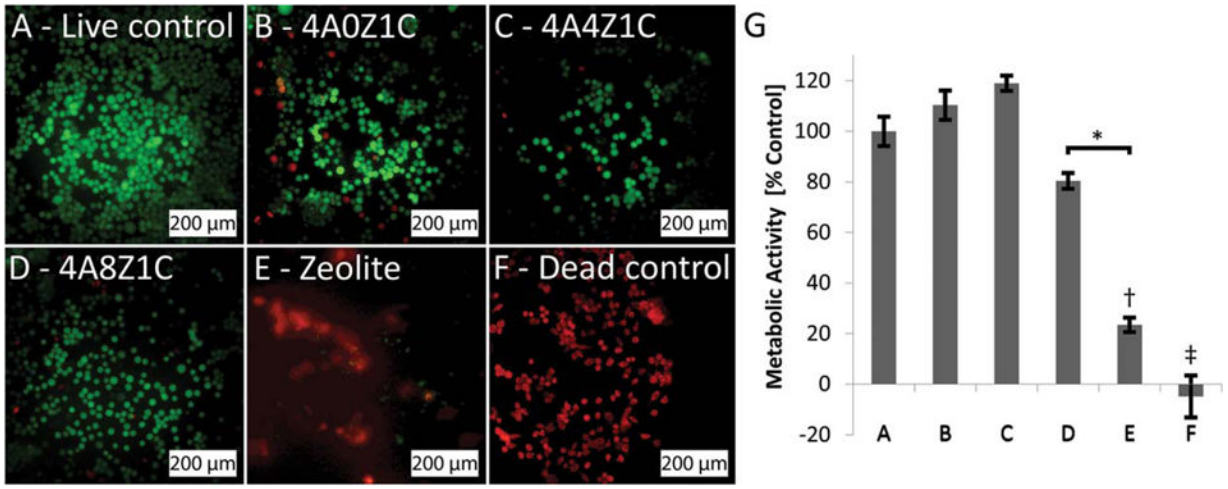

FIGURE 7.

Live/Dead and MTS of murine fibroblast L929 cells. Dead cells fluoresced red against live cells, which fluoresced green. (B) 4A0Z1C beads, (C) 4A4Z1C beads, (D) 4A8Z1C beads, and (E) plain zeolite as purchased, are compared to a (A) live control and (F) dead control. Metabolic activity measured by an MTS assay and presented as percent of live control (G) for murine fibroblast L929 cells exposed to each corresponding material composition. * indicates $p < 0.05$ for group D compared with group E. †indicates $p < 0.01$ for group E compared with all other groups except for group F. ‡ indicates $p < 0.001$ for group F compared with all other groups except for group E.

TABLE I

Components (% w/v) of Each Synthesized Bead Composition

Sample	Alginate	Chitosan	Zeolite	Acetic Acid	$CaCl_2$
4A0Z1C	4%	1%	–	1%	1%
5A0Z1C	5%	1%	–	1%	1%
6A0Z1C	6%	1%	–	1%	1%
4A4Z1C	4%	1%	4%	1%	1%
4A8Z1C	4%	1%	8%	1%	1%
4A0Z0C	4%	–	–	1%	1%
4A0Z0C nonacid	4%	–	–	–	1%